Atomistic study of hydrogen distribution and diffusion around a (112)[111] edge dislocation in alpha iron

Shinya Taketomi[a,b,*], Ryosuke Matsumoto[a,b], Noriyuki Miyazaki[a,b]

[a] *Department of Mechanical Engineering and Science, Graduate School of Engineering, Kyoto University, Yoshida-Honmachi, Sakyo-ku, Kyoto 606-8501, Japan*

[b] *Visiting Researcher, National Institute of Advanced Industrial Science and Technology (AIST), Tsukuba Central 2, Tsukuba, Ibaraki 305-8568, Japan*

Key words: Hydrogen diffusion, Hydrogen embrittlement, Dislocations, Iron, Atomistic simulations

Abstract

Despite extensive investigations, the distribution of hydrogen around a stress singularity field is not well understood. In this study, we conducted molecular statics (MS) analyses of the hydrogen-trap energy around a (112)[111] edge dislocation in alpha iron. The distribution of hydrogen in crystals is generally assumed to be dominated by hydrostatic stress. However, the MS results indicate that the hydrogen-trap energy is sensitive to shear stress as well as hydrostatic stress, thus indicating that strong trap sites are distributed across a wide range on the slip plane around the dislocation core. We also performed molecular dynamics simulation of

hydrogen diffusion, and revealed the anisotropic diffusion behaviour of hydrogen around the dislocation core.

1. Introduction

In order to ensure the safe use of hydrogen as an energy medium and source, there is a pressing need to establish the technologies needed for generating, transporting and storing hydrogen. Hydrogen embrittlement is a well-known phenomenon where hydrogen lowers the strength of materials. Despite extensive investigations for over a century, the role of hydrogen in materials remains unclear.

A well-known effect of hydrogen on mechanical properties is the reduction in ductility [1]. Hence, the interactions between dislocations and hydrogen atoms have been considered as an important factor in understanding the hydrogen embrittlement process [2-6]. In order to reveal the fundamental effects of hydrogen on dislocation activity, it is necessary to obtain precise estimates of local distribution and the concentration of hydrogen around a dislocation.

Measurements of hydrogen in metals have been performed recently by secondary ion mass spectroscopy (SIMS), hydrogen microprint technique (HMPT) or thermal desorption analysis (TDA) [7]. However, because of high diffusivity and extremely low concentration of hydrogen, identification of hydrogen distribution in metals, and in particular, the estimation of hydrogen occupation sites around a stress singularity field (i.e. crack-tip and dislocations) is difficult. To address this problem, a numerical analysis is considered to be the most effective method [4, 8-10]. Since the interstitial hydrogen atoms dilate the crystal lattice, they are assumed to interact with

hydrostatic stress. Hence, the previous analyses assumed that the hydrogen distribution follows the hydrostatic stress distribution, and that the gradient of hydrostatic stress acts as a driving force for hydrogen diffusion. Moreover, most analyses were based on continuum theory of elasticity; therefore, they did not take the dislocation core structure into consideration. To further understand the hydrogen distribution and diffusion around dislocations, an analysis based on atomistic model is considered to be effective.

In this study, the hydrogen distribution around an (112)[111] edge dislocation in alpha iron is investigated using an atomistic model. In general, alpha iron has (110)[111] and (112)[111] main slip systems. Bastien et al. experimentally determined that the (112) slip plane only shows distortion in the presence of hydrogen, and the materials without the (112) activated slip were reported to be insensitive to hydrogen [11]. Therefore, this study deals with edge dislocation on a (112) plane. The material chosen for this study is alpha iron because pure-iron was also reported to be sensitive to hydrogen [12, 13], and its alloys (such as carbon steel and stainless steels) are expected to serve as hydrogen storage and piping components due to their low costs.

2. Analytical

2.1 Analysis model

The crystallographic orientation of the analysis model is shown in Fig. 1. The slip occurs on the (112) plane, and the slip direction [111] was set along the *x* axis. Periodic boundary conditions were applied along the *x* and *z* axes. In order to introduce an edge dislocation, an atomic plane shown in Fig. 1 was removed, and then the relaxation of atomic structure was performed by the conjugate gradient (CG) method. During the structural relaxation process, the movement of atoms along the *y* axis was

fixed and then compression was applied along the *x* axis in order to fill the removed plane. After that, the unit cell size and the atomic positions were relaxed until the *x* axis stress (σ_{xx}) decreased sufficiently. The analysis system contains 8,054 iron atoms, and the dimensions of the unit cell are 11.05, 4.91 and 2.02 nm along the *x*, *y* and *z* axes, respectively. In this system, the dislocation density is approximately 0.018 nm^{-2}. Three atomic layers at the top and bottom of the unit cell were considered as boundary layers and fixed.

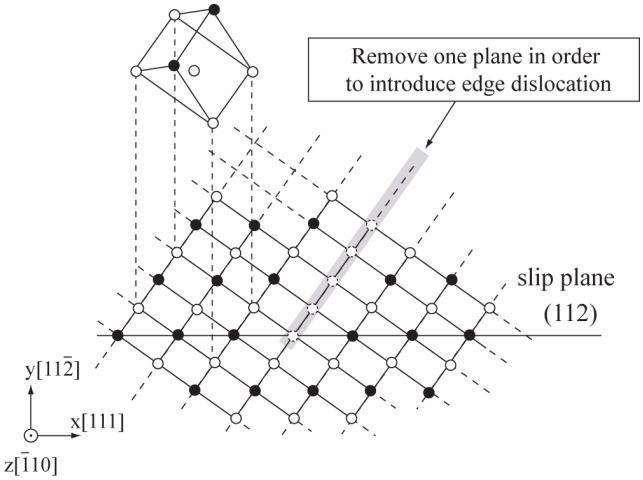

Fig. 1 Simulation model and coordinate system: The (112)[111] edge dislocation was introduced on the *xz* plane.

2.2 Interatomic potential

Analytical results obtained by atomistic simulation are strongly influenced by the characteristics of interatomic potential; therefore, the choice of the interatomic potential that determines the atomic interaction is extremely important. Recently, the embedded atom method (EAM) potential developed by Ruda et al. [14], the Morse-type potential developed by Hu et al. [15] and the EAM potential developed by Wen et al. [16] have been proposed to express the iron and hydrogen (Fe–H) system. In this paper,

EAM potential developed by Wen et al. was adopted. The interaction between Fe–Fe was described using the EAM potential developed by Johnson and Oh [17]. The Fe–H interaction was expressed using a Morse-type function, and the H–H interaction was described using the EAM potential developed by Baskes et al. [18, 19]. The EAM potential developed by Wen et al. was found to be the most reliable, because it accurately represents the material constants (e.g. heat of solution, elastic constants and stacking fault energy) [20].

2.3 Hydrogen occupation sites at the initial state

There are two types of hydrogen occupation sites within the undeformed bcc lattice as shown in Fig. 2. One is the tetrahedral site (T site) and the other is the octahedral site (O site). Both occupation sites have an anisotropic geometry illustrated in Fig. 2 (a) and (b). The T site is the more stable occupation site for a hydrogen atom in most bcc metals [21]. However, it was reported that the O site becomes more stable under the monoaxial tensile condition for bcc-structured metal [22]. Here we are dealing with the disordered crystalline region near the dislocation core, and therefore, a hydrogen atom within both T and O sites is taken into consideration. Here, T sites within the perfect bcc lattice correspond to the vertices of a Voronoi polyhedron, as shown in Fig. 2(c). Moreover, the O sites are located at the center of square on the polyhedron surfaces. Using these rules, hydrogen occupation sites were estimated under lattice distortion conditions. Although, these sites do not exactly correspond to the T and O sites in the significantly distorted lattice, for convenience, we will hereafter refer to these sites as T and O sites, respectively.

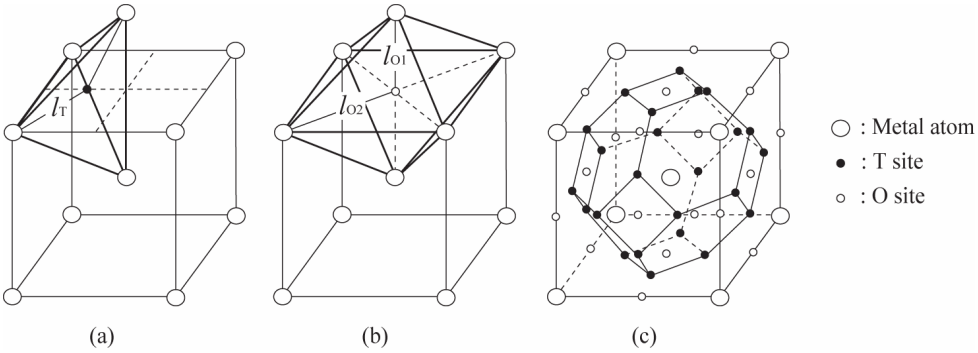

Fig. 2 Hydrogen occupation sites in a bcc lattice: (a) Geometry of the T site. Here, l_T is the distance between the neighbouring atoms and $l_T = \sqrt{5}/4 \times a$, where a is the lattice constant. (b) Geometry of the O site. $l_{O1} = 1/2 \times a$ and $l_{O2} = \sqrt{2}/2 \times a$. (c) T sites correspond to the vertices of a Voronoi polyhedron and O sites are located at the center of the squares on the polyhedron surfaces.

3. Results and discussion

3.1 Atomistic structure of the dislocation

The atomic configuration around the dislocation core after the relaxation is shown in Fig. 3. The crystalline structure was detected using common neighbor analysis (CNA) [23]. In this figure, bcc-structured atoms are shown as white and the others as black points. According to the molecular dynamics (MD) study for alpha iron using the Finnis-Sinclair (FS) potential [24], the (112)[111] edge dislocation core was reported to have a width of about 4*b,* where *b* is Burger's vector [25]. The atomistic structure of the edge dislocation in this analysis also has a width of about 4*b* along the negative *x* axis, pointing from the initial dislocation-core position. Here we consider the crystalline disordered region, denoted by the black dotted circle in Fig. 3, as the dislocation core.

Distribution of hydrostatic (σ_h) and shear stresses (τ_{xy}) around the edge dislocation, which were exerted on each atom, obtained by the CG method, are shown

in Fig. 4 (a) and (b), respectively. The illustrated regions here are the same as those in Fig. 3. These distributions are in good agreement with the results obtained from the theory of elasticity [26].

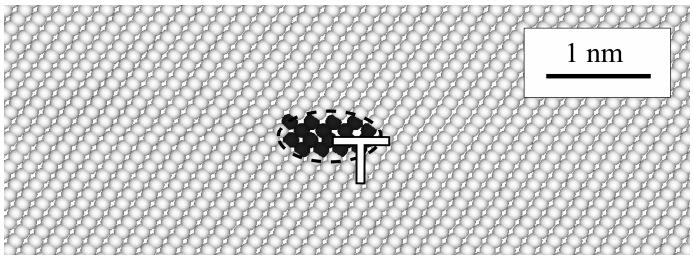

Fig. 3 Atomistic structure around the (112)[111] edge dislocation: white points correspond to bcc structure and black to non-bcc structures.

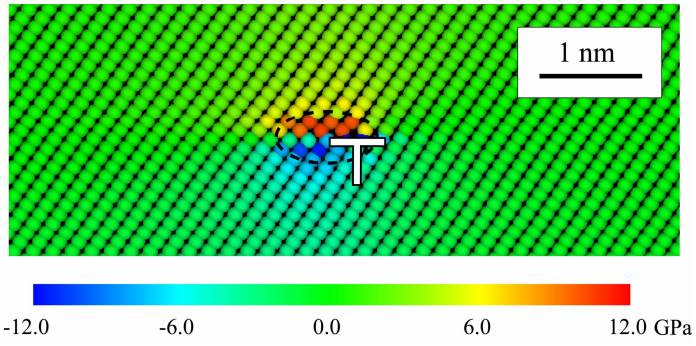

(a) Hydrostatic stress (σ_h).

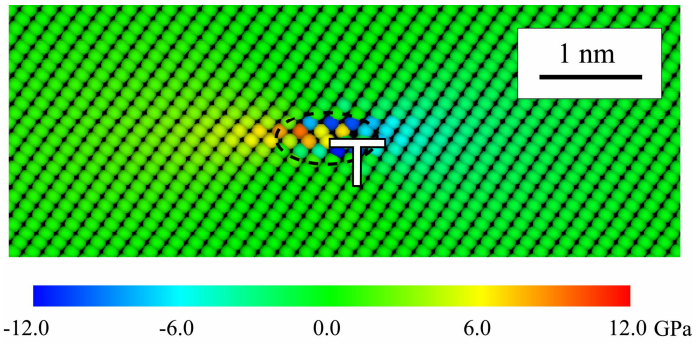

(b) Shear stress (τ_{xy}).

Fig. 4 Stress distributions around the (112)[111] edge dislocation.

3.2. Distribution of hydrogen-trap energy around the edge dislocation

A hydrogen atom was introduced into each T and O sites detected by Voronoi tessellation. The positions of the Fe and H atoms were then relaxed to minimize the total potential energy by the CG method. The hydrogen-trap energy at each occupation site is shown in Fig. 5. The estimated region shown here is the same as that shown in Fig. 3. Here, the hydrogen-trap energy, $\Delta E_{\mathrm{d}}(\boldsymbol{r})$, at the hydrogen occupation site $\boldsymbol{r}$, is calculated using the following equation:

$$\Delta E_{\mathrm{d}}(\boldsymbol{r}) = -\left[\left\{\Phi_{\mathrm{d,H}}(\boldsymbol{r}) - \left(\Phi_{\mathrm{d}} + \frac{1}{2}\Phi_{\mathrm{H2}}\right)\right\} - H^{\mathrm{T}}\right], \tag{1}$$

where, $\Phi_{\mathrm{d,H}}(\boldsymbol{r})$ is the potential energy of the system with a hydrogen atom at a trap site located at $\boldsymbol{r}$. Φ_{d} is the potential energy of the system without hydrogen, Φ_{H2} is the potential energy of the hydrogen molecule and H^{T} is the heat of solution of the hydrogen atom on the T site in the alpha iron lattice, with value equal to 0.45×10^{-19} J. The position of initial dislocation core ($\perp$) and the dislocation core region (given by dotted line in Fig. 3) are also shown in the figure. Trap sites with strong hydrogen-trap energy are distributed around the dislocation core, and the maximum hydrogen-trap energy in the dislocation core is about 7×10^{-20} J. This value lies in the range of experimental estimations (3.19×10^{-20} J [27] and 9.95×10^{-20} J [28]). The detailed trap-energy distribution along the slip plane of 0.5 nm width (region C in Fig. 5) is shown in Fig. 6 (a), and the trap-energy distribution in region D in Fig. 5 is also shown in Fig. 6 (b). Figure 6 (b) shows the maximum hydrogen-trap energy in region A, which is approximately equal to 2.0×10^{-20} J except the dislocation core. Meanwhile, hydrogen-trap energy at the region B is much stronger than that in region A.

The results could not be predicted by the theory of elasticity that hydrogen and

dislocation interact mechanically as a result of lattice dilatation caused by solute–hydrogen atom because high hydrostatic stress was not observed in region B. Typical stress exerted on region B is shear stress τ_{xy}, as shown in Fig. 4 (b); therefore, a relationship between hydrogen-trap energy and shear stress is assumed. Furthermore, this result suggests that hydrogen atoms accumulate on the slip plane around the dislocation core.

The stripe shaped trap-energy distribution is also observed as indicated by the arrows in Fig. 5. The energy differences between the peaks and valleys in the stripe pattern are larger than the difference of heat of solution between the T and O sites in the absence of strain (0.58×10^{-20} J).

There is a difference in hydrogen occupation site distribution in the left and right side of the dislocation core, as shown in Fig. 5. Therefore, the hydrogen atoms are supposed to migrate to another occupation site from the sites at which they are introduced initially during the calculation. In order to investigate the hydrogen-trap energy of exact T/O sites around the dislocation core, the hydrogen atom is fixed at the site of initial introduction and only the positions of Fe atoms are relaxed using CG method. Hydrogen-trap energy for each T and O site estimated by equation (1) is shown in Fig. 7 (a) and (b), respectively. Even in the same T and/or O site, hydrogen-trap energy shows different characteristics depending on the occupation sites (indicated by arrows in Fig. 7 (a) and (b)). Hydrogen atom is strongly trapped at the dislocation core for both the sites; however, T sites show strong trap-energy at region A, and O sites show strong trap-energy at region B.

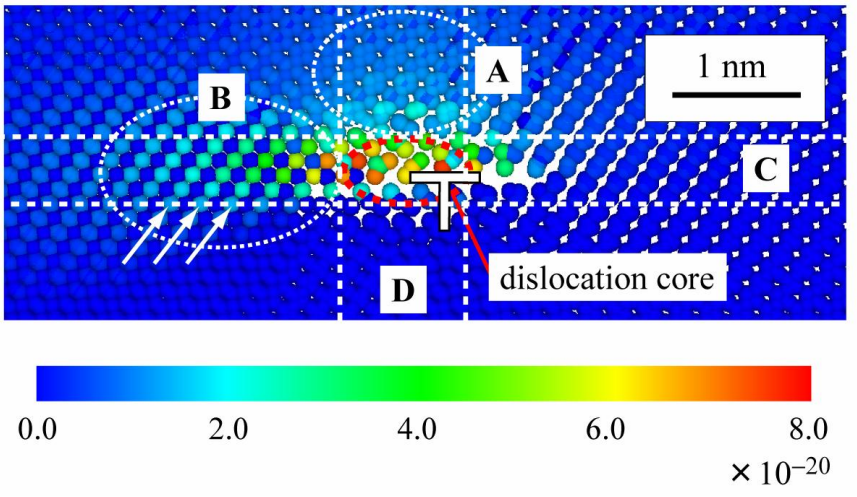

Fig. 5 Distribution of hydrogen-trap energy around a dislocation (Both Fe and H atoms were relaxed).

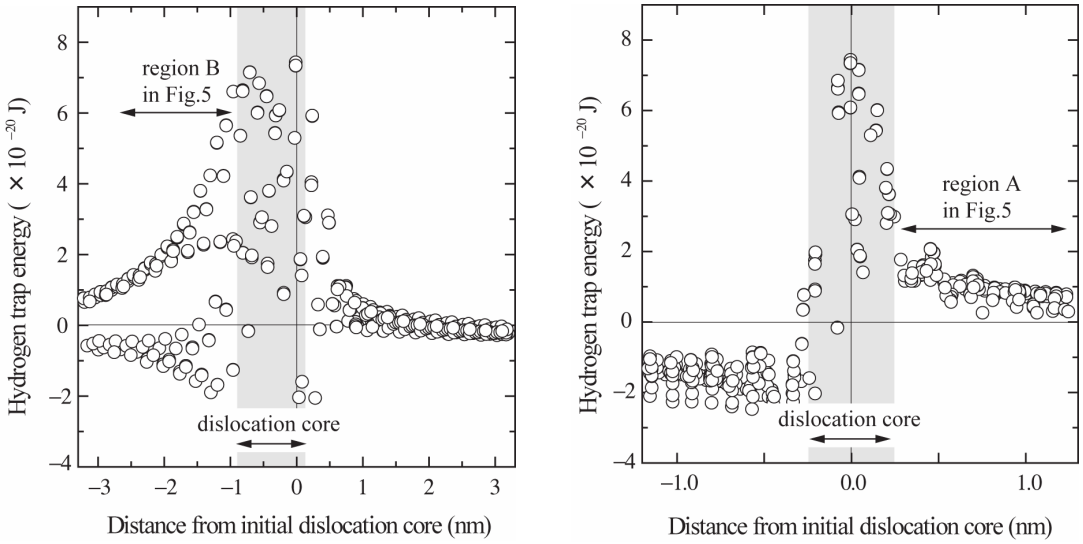

(a) Region C (b) Region D

Fig. 6 Hydrogen trap-energy distribution in cross sections.

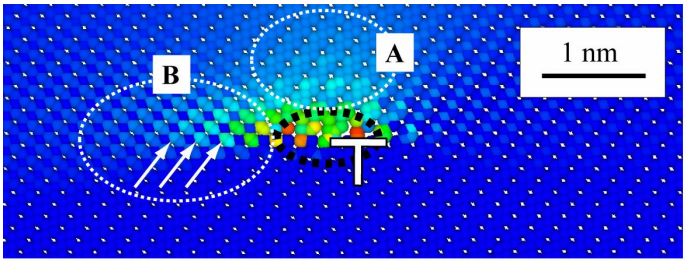

(a) T site

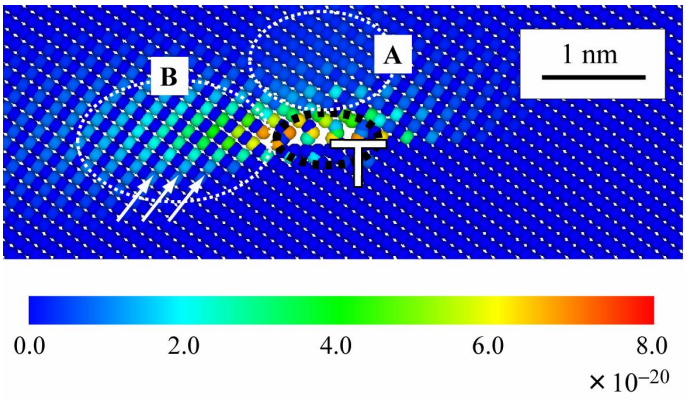

(b) O site

Fig. 7 Distribution of hydrogen-trap energy at each site (H atom is fixed and only Fe atoms are relaxed): (a) hydrogen atoms at T sites and (b) hydrogen atoms at O sites.

In order to investigate the hydrogen-trap energy for T and O sites under shear stress, 7,038 Fe atoms were arranged along the crystal orientations as shown in Fig. 1. Periodic boundary conditions were applied along the x and z axes, three atomic layers at the top and bottom of the simulation model were fixed, and displacements corresponding to simple shear γ were given along the [111] direction. The hydrogen-trap energy under simple shear strain $\Delta E_s(\gamma, \boldsymbol{r})$ for each occupation site is shown in Fig. 8. Here, $\Delta E_s(\gamma, \boldsymbol{r})$ was defined as the difference of the heat of solution of hydrogen in a lattice with and without shear deformation. The expression used in the calculation is given by

$$\Delta E_{\mathrm{s}}(\gamma,\boldsymbol{r}) = -\left[\left\{\Phi_{\mathrm{H}}(\gamma,\boldsymbol{r}) - \left(\Phi(\gamma) + \frac{1}{2}\Phi_{\mathrm{H2}}\right)\right\} - H^{\mathrm{T}}\right], \tag{2}$$

where $\Phi_{\mathrm{H}}(\gamma, \boldsymbol{r})$ and $\Phi(\gamma)$ are the potential energies of the system under simple shear γ with and without a hydrogen atom, respectively.

The effect of shear strain on the hydrogen-trap energy is also observed in Fig. 8, and it also shows that both the T and O sites reveal two types of hydrogen-trap energies under simple shear for the present crystal orientation. This is assumed to be due to the anisotropic geometry of the hydrogen occupation sites shown in Fig. 2(a) and (b). For convenience, occupation sites that show stronger trap-energies under positive shear stress are called type A, and the sites showing stronger trap-energies under negative shear stress are called type B. The geometrical distribution of type A and B trap sites for T and O sites are shown in Fig. 9. Three-dimensional illustration of the bcc lattice and each hydrogen-occupation site are shown in the upper panel, and its two-dimensional projection onto the *xy* plane is shown in the lower panel. For reference, the relationship between hydrostatic stress and the hydrogen-trap energy is also shown in Fig. 10. Under the tensile hydrostatic stress condition, both T and O sites exhibit stronger trap-energies, as expected, and only one curve is obtained for each occupation site. Comparing Fig. 8 with Fig. 10, it is revealed that the shear stress effect is much stronger than the hydrostatic effect on the trap-energy of an O site type A.

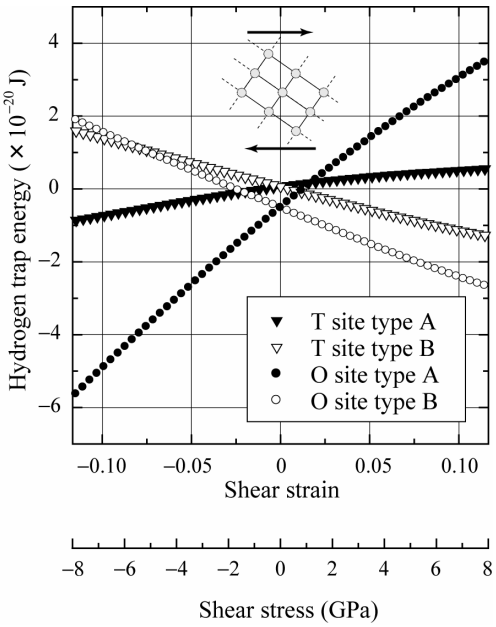

Fig. 8 Relationship between hydrogen-trap energy and applied simple shear: Shear stress calculated by $\tau_{xy} = G\gamma$ is also shown in the horizontal axis. Here, G = 68.6 GPa is used.

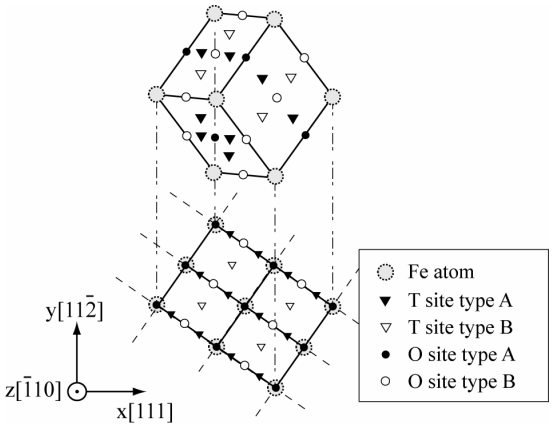

Fig. 9 Illustration of the bcc lattice and hydrogen occupation sites: the three-dimensional illustration is shown in the upper panel and its two-dimensional projection is shown in the lower panel. Each symbol of the occupation sites corresponds to the trap-energy characteristics shown in Figs. 8 and 12.

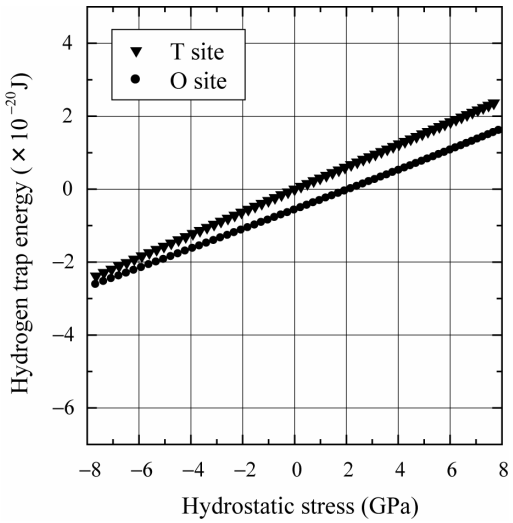

Fig. 10 Relationship between hydrogen-trap energy and applied hydrostatic stress.

3.3 Hydrogen diffusion and trap around the edge dislocation

In order to investigate the hydrogen diffusion and trap behaviours around the edge dislocation, MD simulations were performed. The geometry of the analysis model was the same as that in the MS analyses (Fig. 2), and only one hydrogen atom was introduced at a different position on the slip plane around the dislocation core. The initial positions of the hydrogen atom are denoted in Fig. 11 by the symbol ×.

The reversible reference system propagator algorithm [29] was adopted as a numerical integration method, and the temperature of the system was maintained at 300 K by the velocity scaling method. The boundary atoms, consisting of three atomic layers of the top and bottom of the unit cell, were fixed. The calculations of hydrogen diffusion were conducted for 0.5 ns. At the beginning of the calculation, the unit-cell size of the system was relaxed to minimize the tensile stress (σ_{xx}, σ_{yy}, σ_{zz}) for 10 ps.

The trajectories of each hydrogen atom during the 0.49 ns following the unit-cell size relaxation are shown in Fig. 11. Hydrogen atom (a) diffused primarily through the O site type A (● in Fig. 11) and the T site type A(▼ in Fig. 11). Hydrogen

atoms (b) and (c) were strongly trapped at the O site type A(●), and they did not diffuse to another site during 0.5 ns in this analysis. Hydrogen atoms (d) and (e) are located at the disordered crystalline region near dislocation core, and thus the exact trap-site is difficult to estimate. Both hydrogen atoms were strongly trapped at the occupation sites vicinity of the initial position. Hydrogen atom (f) occupied a T site type B (∇ in Fig. 11) or an O site type B (○ in Fig. 11), and it did not show long range diffusion. Finally, hydrogen atom (g) diffused through a T site type B(∇), O site type B(○) and T site type A(▼), and it was the most mobile among all hydrogen atoms.

The dominant stress along the slip plane is shear stress τ_{xy}, as shown in Fig. 4. The distribution of stable hydrogen-trap sites is shown in Fig. 12 which results from the dependence of the hydrogen-trap energy on shear stress (Fig. 8) and shear stress around the dislocation (Fig. 4 (b)). At the initial location of the hydrogen atom (a), about 1.9 GPa of shear stress is applied, and therefore an O site type A (●) and T site type A (▼) show strong trap-energies, as shown in Fig. 12 (I). At the initial location of hydrogen atoms (b) and (c), the shear stress is greater than 3.2 GPa, and therefore, an O site type A (●) shows an extremely strong hydrogen trap-energy, as shown in Fig. 12 (II). Hydrogen atom (f) was initially located at the from –4 to –6 GPa lattice site, and therefore the T site type B(∇) and O site type B (○) have the same level of hydrogen trap energies, as shown in Fig. 12 (III). Finally, at the initial location of hydrogen atom (g), about –2.5 GPa of shear stress was applied, and therefore a T site type B(∇) and an O site type B(○) and T site type A(▼) could be hydrogen trap sites as shown in Fig. 12 (IV). These results are in good agreement with the trajectories of the hydrogen diffusion path for each H atom obtained by molecular dynamics analyses.

Since hydrogen atoms (b)–(f) did not diffuse in this analysis, the high hydrogen

concentration region is supposed to be formed within about 3 nm width along the slip plane. These results suggest that a high hydrogen-concentration plane can be formed along the piled-up dislocations to obstacles (e.g. grain boundary and inclusion), and that such a region might become a nucleation site for a crack or void. In addition, hydrogen atoms (a) and (g) revealed anisotropic diffusion trajectories; in particular, in the case of hydrogen atom (a) the anisotropic diffusion was remarkable. These atoms diffused through specific layers of the occupation sites (indicated by arrows in Fig. 12), and rarely changed the diffusion layer. Consequently, the hydrogen-diffusion coefficient along the direction of dislocation motion could be remarkably low. This result suggests that the critical velocity below which hydrogen atoms can follow the motion of dislocation is reduced; i.e. the hydrogen-drag ability of dislocation is reduced. Although the quantum diffusion caused by the tunnel effect also contributes to hydrogen diffusion, it is sensitive to the distance between the sites. Fig. 12(I) clearly shows that the distances between the diffusion layers are sufficiently far, and thus, the hydrogen diffusion across the layers is not easy, even when quantum effects are taken into consideration.

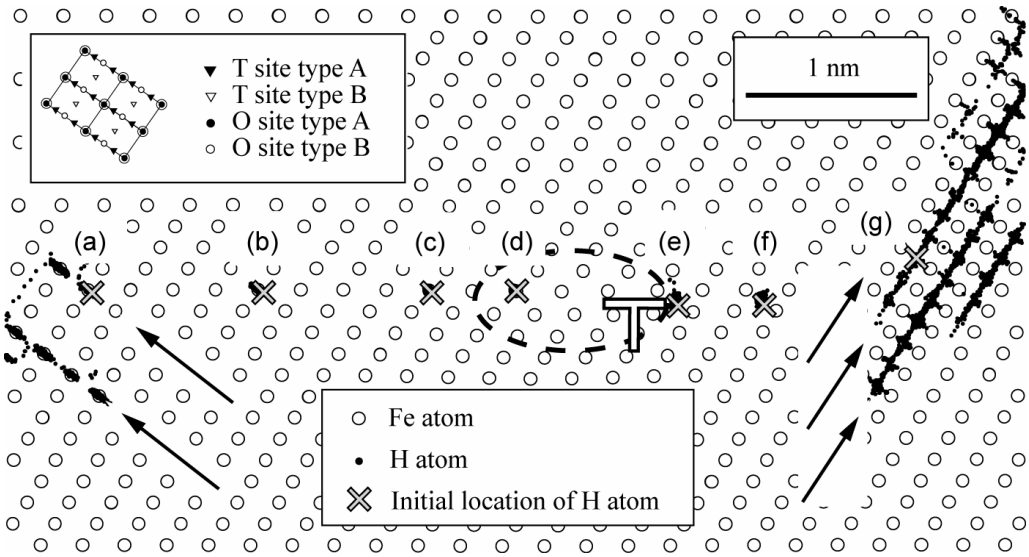

Fig. 11 Trajectories of hydrogen diffusion around the dislocation. The initial hydrogen location after the relaxation is marked by the symbol ×.

(For the molecular dynamics results, the temperature is maintained at 300 K for 0.49 ns)

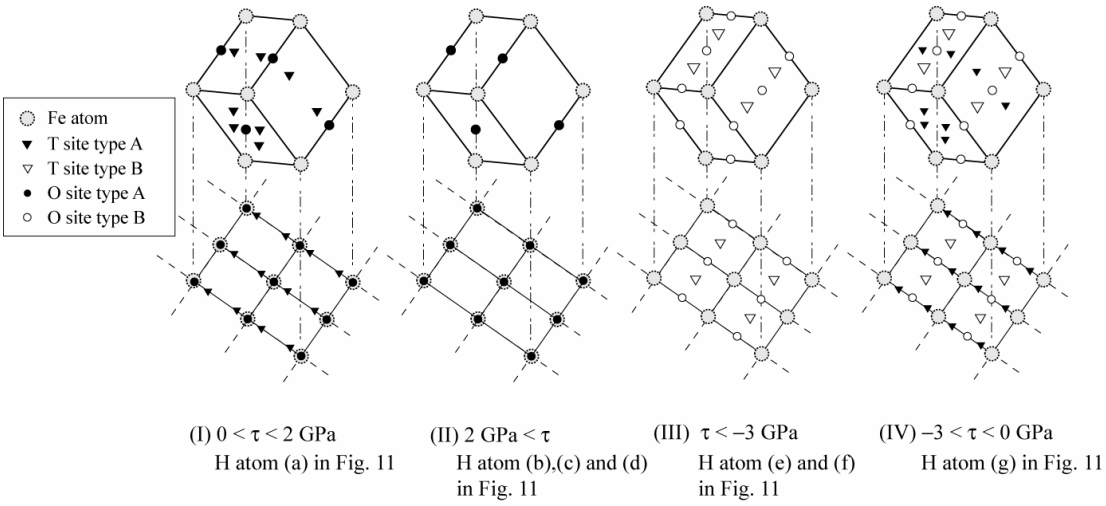

Fig. 12 Hydrogen occupation sites under various shear stress conditions:

(I): 0–2 (II): 2–8 (III): from –8 to –3 (IV): from –3 to 0 GPa

4. Conclusions

Hydrogen occupation sites and diffusion behaviour around an edge dislocation on a (112) slip plane in alpha iron was investigated using atomistic simulations, and the following conclusions were obtained.

(1) Hydrogen atoms exist stably on the edge dislocation core and the exact slip plane, and the results suggest that high hydrogen concentration is formed along the slip plane near the dislocation core.
(2) Hydrogen distribution is also sensitive to shear stress for the crystal orientation analysed here, and therefore, the local hydrogen distribution can not be explained using only the hydrostatic stress distribution, even for a crystalline structure.
(3) The hydrogen-trap energy shows different characteristics that depend on the crystallographic position, even for the same T and O occupation sites. This nature leads to the characteristic distribution and diffusion behaviour of hydrogen atoms around the dislocation core, i.e. stripe pattern of trap energy distribution and layer by layer diffusion of hydrogen.

These results suggest that hydrogen is trapped with the help of shear stress, and therefore, screw dislocations are also supposed to interact with hydrogen, except at the dislocation core, and that hydrogen concentration around the mode II or III crack-tip could also increase. We note that, in general, the analysis based on the atomistic model is strongly affected by the interatomic potential. However, the shear stress contribution on the hydrogen trap-energy does not disappear. In order to perform quantitative analysis of materials in nature, *ab-initio* estimation of the effect of strain on the trap

energy, similar to that shown in Figs. 8 and 10, is necessary, and we can obtain the distribution of hydrogen-trap energies around the dislocation core by adapting these *ab-initio* results to the elastic field obtained using the theory of elasticity.

Acknowledgements

This research was performed as part of the Fundamental Research Project on Advanced Hydrogen Science funded by the New Energy Development Organization (NEDO). The research has also been partially supported by the Ministry of Education, Science, Sports and Culture's Grant-in-Aid for Young Scientists (A).

References

[1] Han G, He J, Fukuyama S, Yokogawa K. Acta mater 1998;46,13:4559.

[2] Beachem CD. Metall Trans 1972;3,2:437.

[3] Birnbaum HK, Robertson IM, Sofronis P, Teter D. Mechanisms of hydrogen related fracture – a review. In: Magnin T, editor. Mater sci forum, London (UK): Institute of Materials, 1997. p.172.

[4] Sofronis P, Birnbaum HK. J mech phys solids 1995;43, 1:49.

[5] Ferreira PJ, Robertson IM, Birnbaum HK. Acta mater 1999;47,10:2991.

[6] Taketomi S, Matsumoto R, Miyazaki N. J mater sci 2008;43, 3: 1166.

[7] Kawamoto K, Oda Y, Noguchi H, Fujii H, Izumi T, Itoh G. T jpn soc mech eng, A 2007;73,731:36 (in Japanese).

[8] Krom AHM, Koers RWJ, Bakker A. J mech phys solids 1999;47,971:21.

[9] Yokobori Jr. AT, Chinda Y, Nemoto T, Satoh K, Yamada T. Corros science 2002;44,407:17.

[10] Kotake H, Matsumoto R, Taketomi S, Miyazaki N. Int j pres ves pip 2008

(accepted).

[11] Bastien P, Azou P, Compt. Rend. Acad. Sci. 1951;232:1845.

[12] Kimura A, Matsui H, Kimura H. Mater sci eng1983;58:211.

[13] Matsui H, Kimura H, Moriya S. Mater sci eng1979;40:207.

[14] Ruda M, Farkas D, Abriata J. Phys rev B 1996;54,14:9765.

[15] Hu Z, Fukuyama S, Yokogawa K, Okamoto S. Mod sim mater sci eng 1999;7,4:541.

[16] Wen M, Xu XJ, Fukuyama S, Yokokawa K. J mater res 2001;16,12:3496.

[17] Johnson RA, Oh DJ. J mater res 1989;4,5:1195.

[18] Angelo JE, Moody NR, Baskes MI. Mod sim mater sci eng 1995;3:289.

[19] Baskes MI, Sha X, Angelo JE, Moody NR. Mod sim mater sci eng 1997;5:651.

[20] Matsumoto R, Inoue Y, Taketomi S, Miyazaki N. Comp mater sci(submitted).

[21] Fukai Y, Tanaka K, Uchida H. In: Hydrogen and metal: Uchida Rokakuho Publishing 1998:56 (in Japanese).

[22] Fukai Y. J less-common metals 1984;101:1.

[23] Honeycutt JD, Andersen HC. J phys ch 1987;91,19:4950.

[24] Finnis MW, Sinclair JE. Philos mag A 1984;50,1:45.

[25] Nakatani A, Kitagawa H, Nakatani K. J soc mater sci, Japan 1997;46,6:625(in Japanese).

[26] Steeds JW. Introduction to Anisotropic Elasticity Theory of Dislocations, Oxford (UK): Clarendon Press, 1973 p. 178.

[27] Choo WY, Lee JY. Metall trans A 1982;13,1:135.

[28] Kummick AJ, Johnson HH. Acta Metall 1980;28:33.

[29] Tuckerman M. J chem phys 1992;97:1990.